Hurricane Surface Wind Measurements from an Operational Stepped Frequency Microwave Radiometer

Eric W. Uhlhorn*
NOAA/AOML/Hurricane Research Division, Miami, FL

Peter G. Black
NOAA/AOML/Hurricane Research Division, Miami, FL

James L. Franklin
NOAA/NWS/TPC/National Hurricane Center, Miami, FL

Mark Goodberlet
ProSensing, Inc., Amherst, MA

James Carswell
Remote Sensing Solutions, Inc., Barnstable, MA

Alan S. Goldstein
NOAA/OMAO/Aircraft Operations Center, Tampa, FL

Submitted to:
Monthly Weather Review

November 30, 2006

*4301 Rickenbacker Cswy.; Miami, FL 33149; email: Eric.Uhlhorn@noaa.gov

Abstract

For the first time, the NOAA/Aircraft Operations Center (AOC) flew Stepped Frequency Microwave Radiometers (SFMR) on both WP-3D research aircraft for operational hurricane surface wind speed measurement in 2005. An unprecedented number of major hurricanes provided ample data to evaluate both instrument performance and surface wind speed retrieval quality up to 70 $\mathrm{m\,s^{-1}}$ (Saffir-Simpson category 5). To this end, a new microwave emissivity/wind speed model function based on estimates of near-surface winds in hurricanes by GPS dropwindsondes is proposed. For practical purposes, utilizing this function removes a previously-documented high bias in moderate SFMR-measured wind speeds (10–50 $\mathrm{m\,s^{-1}}$), and additionally corrects an extreme wind speed (>60 $\mathrm{m\,s^{-1}}$) systematic underestimate.

The AOC operational SFMRs yield retrievals precise to within ∼2% at 30 $\mathrm{m\,s^{-1}}$, which is a factor of two improvement over the NOAA Hurricane Research Division's SFMR, and comparable to the precision found here for GPS dropwindsonde near-surface wind speeds. A small (1.6 $\mathrm{m\,s^{-1}}$), but statistically significant, overall hight bias was found for independent SFMR measurements utilizing emissivity data not used for model function development. Across the range of measured wind speeds (10–70 $\mathrm{m\,s^{-1}}$), SFMR 10-s averaged wind speeds are within 4 $\mathrm{m\,s^{-1}}$ (rms) of the dropwindsonde near-surface estimate, or 5–25% depending on speed. However, an analysis of eyewall *peak* wind speeds indicates an overall 2.6 $\mathrm{m\,s^{-1}}$ GPS low bias relative to the peak SFMR estimate on the same flight leg, suggesting a real increase in the maximum wind speed estimate due to SFMR's high-density sampling. Through a series of statistical tests, the SFMR is shown to reduce overall bias in the peak surface wind speed estimate by ∼50% over the current flight-level wind reduction method, and is comparable at extreme wind speeds.

The updated model function is demonstrated to behave differently below and above the hurricane wind speed threshold ($\sim$32 $\mathrm{m\,s^{-1}}$), which may have implications for air-sea momentum and kinetic energy exchange. The change in behavior is at least qualitatively consistent with recent laboratory and field results concerning the drag coefficient (C_d) in high wind speed conditions, which show a fairly clear "leveling-off" of C_d with increased wind speed above $\sim$30 $\mathrm{m\,s^{-1}}$. Finally, a composite analysis of historical data indicates the earth-relative SFMR peak wind speed is typically located in the hurricane's right-front quadrant, consistent with previous observational and theoretical studies of surface wind structure.

1. Introduction

Estimating hurricane surface wind distributions and maxima is an operational requirement of the Tropical Prediction Center/National Hurricane Center (TPC/NHC), and emergency management decisions rely on coastal watches and warnings issued by NHC based partly on observed winds. Surface wind speed estimates by NHC are determined largely from extrapolated aircraft flight-level wind data. In 1997, GPS dropwindsondes (Hock and Franklin 1999) first demonstrated the ability to provide *in situ* measurements of hurricane surface wind velocities, most importantly in the inner core, and recent work utilizing these measurements has improved the accuracy of extrapolations (Franklin et al. 2003).

Since 1984, the NOAA/Hurricane Research Division's (HRD) Stepped Frequency Microwave Radiometer (HSFMR) has flown on one of two NOAA WP-3D research aircraft to estimate hurricane surface wind speeds (Uhlhorn and Black 2003). Beginning in 2004, a re-designed SFMR was flown on one WP-3D aircraft for operational surface wind speed measurements. After procedural testing during 2004, both WP-3Ds had operational SFMRs installed in 2005 (SFMR-2 and SFMR-3). The unusually active 2005 Atlantic hurricane season provided ample opportunity to evaluate the SFMRs' performances over the entire range of expected surface wind speeds (10–70 $\mathrm{m\,s^{-1}}$). In particular, extreme wind speed ($>$60 $\mathrm{m\,s^{-1}}$) measurements were obtained from flights into Saffir-Simpson category-5 hurricanes Katrina and Rita.

The SFMR measures nadir brightness temperature (T_B) at six C-band frequencies, and a retrieval algorithm uses a geophysical model function (GMF) relating surface emissivity and wind speed to produce surface wind speed estimates along the flight track. Previous emissivity/wind speed models used in microwave radiometry applications have been developed for winds $<$25 $\mathrm{m\,s^{-1}}$ (Goodberlet et al. 1989; Wentz et al. 1986; Wentz 1983; Webster et al. 1976), or either relied upon or were validated against aircraft flight-level high-wind data extrapolated to the sea surface (Uhlhorn and Black 2003; Tanner et al. 1987; Black and Swift 1984; Swift et al. 1984; Jones et al. 1981). All of these methods resulted in uncertainty about the

retrieved hurricane surface wind speed, especially under extreme conditions. The current emissivity/wind speed GMF development takes an approach decidedly different from the previous methodology; recent improvements to the GPS dropwindsondes have increased the availability of surface wind speed estimates in extreme conditions, and are utilized here to re-evaluate the SFMR GMF.

Recent studies (Dunion et al. 2003; Franklin et al. 2003; Powell et al. 2003, 1999) indicate boundary-layer models used to extrapolate flight-level wind speeds (Powell 1980; Deardorff 1972; Cardone 1969; Blackadar 1965) show a tendency to underestimate surface wind speeds $>50\ \mathrm{m\,s^{-1}}$. Anecdotal evidence has also suggested that the SFMR underestimated surface wind speeds in similar conditions. Utilizing the previous GMF, comparisons of SFMR-derived wind speeds with GPS surface-reduced, 0–500 m layer-averaged winds indicated no such tendency (Uhlhorn and Black 2003), but, in fact, very little *in situ* data were available at speeds above $50\ \mathrm{m\,s^{-1}}$. However, when compared with surface-adjusted lowest 150 m layer-averaged winds obtained in 2004, a low bias in SFMR retrievals became apparent at extreme wind speeds. With the recent surge in particularly intense hurricanes, analyzing and correcting this anomalous behavior has become critical. During 2005, a large dataset of contemporaneous SFMR and GPS dropwindsonde observations was obtained, resulting in significant improvement to the empirically-derived SFMR emissivity/wind speed GMF, most notably at extreme wind speeds. This new model function has been implemented operationally beginning in 2006.

This paper is organized as follows: Section 2 presents the methodology for the new SFMR GMF development using measurements obtained from one of the two AOC SFMRs. Section 3 contains an evaluation of retrievals computed using the proposed GMF for all three SFMRs operated during 2005. In Section 4, SFMR overall wind speed measurement uncertainty is analyzed relative to other surface wind estimates, and peak surface wind speed accuracy and expected azimuthal location are identified. Section 5 discusses physical implications for the results, and Section 6 contains concluding remarks.

2. Empirical Model Function Development

In 2005, for the first time, the NOAA/Aircraft Operations Center (AOC) operated a wing pod-mounted SFMR on each of the two WP-3Ds (N42RF and N43RF). The AOC SFMR (designed and built by ProSensing, Inc. of Amherst, MA) includes improved calibration hardware, with fast switching between antenna and calibration loads, and an internal cold load for improved calibration stability and lower ΔT_B noise level (Goodberlet and Mead 2006). Additionally, N43RF also carried HRD's fuselage-mounted research SFMR. Brightness temperature data, calibrated in weak wind speed ($<5\ \mathrm{m\,s^{-1}}$) conditions, were obtained on over 70 flights between the two aircraft. From a subset of T_B measurements, the sea surface emissivity is computed, and regressed with surface (assumed 10 m) wind speed measurements from GPS dropwindsondes. Due to the significant number of extreme wind speeds observed from N43RF, data from this SFMR (SFMR-3) are utilized.

a. Emissivity data

The SFMR algorithm, as detailed in Uhlhorn and Black (2003), uses a forward radiative transfer model (Ulaby et al. 1981) to estimate the atmospheric contribution to the total brightness temperature measured by the SFMR. The intervening atmosphere assumes tropical thermodynamic structure (Jordan 1958), which introduces negligible error under nearly all flight conditions. Given a calibrated SFMR T_B measurement, the sea-surface emissivity, ϵ, may be computed by rearranging the brightness temperature equation (Equation A6 of Uhlhorn and Black (2003)):

$$\epsilon = \frac{T_B - \tau_r \tau_a T_{sky} - T_{up}}{\tau_r \tau_a (T_s - T_{sky})}, \tag{1}$$

where τ_r and τ_a are the transmissivities of the rain column and atmosphere below the aircraft, respectively, T_{sky} is the sky brightness temperature which is the sum of the downwelling atmopheric contribution and cosmic source, T_{up} is the upwelling atmospheric brightness temperature, and T_s is the sea surface temperature.

In tropical cyclones (TCs), rainfall is often a significant contributor to the microwave radiation budget. In lieu of accurate, independent estimates of microwave emission by rain below the aircraft, computing the surface emissivity while simultaneously retrieving the rain rate from a set of T_B measurements using the SFMR algorithm is required. The rain absorption coefficient (κ_r) is modeled typically as:

$$\kappa_r = a\, R^b, \tag{2}$$

where R is rain rate in $\mathrm{mm\,hr^{-1}}$, a is a frequency-dependent function (Olsen et al. 1978) and $b = 1.15$[1] (Jiang et al. 2006; Jorgensen and Willis 1982). The nadir transmissivity of the rain column is then calculated as an exponentially-weighted function of the rain-column depth h:

$$\tau_r = \exp(-\kappa_r\, h). \tag{3}$$

For SFMR channel i, the smooth sea surface nadir emissivity, ϵ_{s_i} is computed using the Klein and Swift (1977) algorithm as a function of frequency, sea surface temperature and salinity. Subtracting ϵ_{s_i} from the total emissivity calculated at each channel by Equation 1 gives a remaining frequency-dependent contribution, which may be written as $\epsilon_i^* = \epsilon_{w_i}\,\alpha(f_i)$, where ϵ_{w_i} is the wind-induced emissivity and $\alpha = 1 + 0.15f$ (Webster et al. 1976). A mean ϵ_w is computed from the six channel ϵ_{w_i} measurements,

[1]In Uhlhorn and Black (2003), the exponent was mistakenly presented as $b = 1.35$, which is in fact the C-band radar reflectivity-rain rate relation exponent for hurricanes (Jorgensen and Willis 1982). In practice, using this incorrect value has a negligible effect on the retrieved wind speed, but decreases the retrieved rain rate by roughly a factor of two.

and is averaged over 10 s of data. Typically three measurements are made by each channel during a 10-s period, therefore the average represents 18 independent samples. Figure 1 (left panel) shows a time series of T_B from SFMR-3 for a radial pass through Hurricane Katrina, and the right panel is the time series of corresponding ϵ_w.

[Figure 1 about here.]

b. Surface wind speed data

GPS dropwindsondes (Hock and Franklin 1999) have been deployed from the NOAA WP-3D aircraft for nearly ten years. The dropwindsondes measure atmospheric temperature, pressure and moisture as they descend from the aircraft to the sea surface. Additionally, they yield estimates of the horizontal wind velocity, sampled at 2 Hz, which gives an approximately 5 m vertical resolution. Dropwindsondes reach the sea surface downwind of the launch location, and in hurricanes, may be horizontally advected 10 km or more.

Improvements to the GPS dropwindsonde have increased the availability of 10-m wind speed measurements (U_{10}). However, this single instantaneous measurement may be interpreted as containing "gustiness", and not necessarily representative of the 1-min average, 10-m wind speed required for operations. For this reason, representative near-surface wind speeds are better estimated from a layer-averaged dropwindsonde wind speed. Franklin et al. (2003) estimate the eyewall-mean ratio, $r(z)$, of near-surface wind speed U_{sfc} to the average wind speed in the lowest available 150-m layer, $U_{L150}(z)$, where z is the mean altitude of the layer [2]. Figure 2 indicates the functional form of $r(z)$. For a dropwindsonde that reports wind speeds to the 10-m level, the function gives $r(85\,\mathrm{m}) = 0.83$.

[Figure 2 about here.]

[2] U_{L150} is reported as the "WL150" wind speed in the encoded GPS dropwindsonde message

As an independent check of this near-surface adjustment method, winds measured from GPS dropwindsondes deployed in 2005 are examined. Figure 3 shows the actual 10-m wind speed (U_{10}) measured by the dropwindsonde vs. U_{L150} (left panel) and vs. U_{sfc} (right panel).

[Figure 3 about here.]

The regression line slope ($r = 0.85 \pm 0.03$) in the left panel of Figure 3 indicates that the Franklin et al. (2003) near-surface wind speed adjustment method represents the data used in this analysis within observational error limits. Although the empirical profile-based near-surface adjustment was intended for the hurricane eyewall, no obvious indication exists here that this method cannot be applied throughout the entire distribution of wind speeds.

c. Wind speed/emissivity correlations

Since the GPS dropwindsonde reaches the surface both tangentially and radially downwind of the SFMR footprint, emissivity/wind speed pairings are not co-located. Additionally, data are temporally separated by the time required for the dropwindsonde to fall to the surface, which is typically $<$3 min for a sonde deployed at the 700 mb level. To decide on the optimal SFMR measurement with which to correlate *in situ* winds, two options are considered. Previously, Uhlhorn and Black (2003) paired SFMR wind speed retrievals at the time of dropwindsonde launch with surface wind speed estimates. Alternatively, the possibility of radial displacements affecting the correlation is examined by comparing the SFMR wind speed estimate at the location where the paired measurements' radial distance differences from the hurricane's center are minimized.

Uhlhorn and Black (2003) applied a maximum 15 km launch-to-splash separation distance criterion to reject pairings, although no obvious decorrelation with increased distance was found. Based on analysis of

data from dropwindsondes deployed at ∼700 mb in 2005, the average azimuthal displacement is roughly given by $U_{sfc} \cdot 0.25$ km/($\mathrm{m\,s^{-1}}$), so a sonde typically travels ∼15 km azimuthally when $U_{sfc} = 60\,\mathrm{m\,s^{-1}}$. Since a goal here is to improve SFMR retrievals at surface wind speeds at least this intense, we choose not to apply the previous 15 km criterion.

As a dropwindsonde descends into the hurricane boundary layer, it is typically transported by the frictionally-induced radial flow. Since hurricane winds vary as a function of radius, an inward (outward) radial displacement outside (inside) of the radius of maximum wind could result in an acceleration. The 2005 data indicate a mean inward GPS dropwindsonde launch-to-splash displacement of 0.4 ± 1.9 km, with no significant tendency as a function of U_{sfc}. Correspondingly, the SFMR wind speed at the nearest radial distance from the storm center as the dropwindsonde splash location is very well correlated ($r^2 = 0.99$) with, and unbiased (<0.1 $\mathrm{m\,s^{-1}}$) with respect to, the SFMR measurement at the launch location. The time (10-s) averaged SFMR ϵ_w measurement at the time of dropwindsonde launch is therefore deemed satisfactory, and is correlated with U_{sfc} to develop the GMF. Table 1 lists the 2005 season NOAA WP-3D flights from which measurements are utilized.

[Table 1 about here.]

Samples are next statistically screened for outliers. First, a quadratic function is initially fit to the ϵ_w vs. U_{sfc} data using a robust parameter estimation technique (adapted from Holland and Welsch (1977)) on the basis of the previous quadratic GMF applied in Uhlhorn and Black (2003). Emissivity residuals falling three average deviations outside of the distribution are identified as outliers; a total of six samples were rejected based on this criterion. Two of the rejected data were contaminated by land-based emission (anomalously high emissivities), and the remaining four were likely deployed in high gradient areas where the sonde was transported into, or out of, a higher wind.

The basis for the proposed new GMF is the observation of a non-linear increase in ϵ_w at low to moderate wind speeds (below hurricane force), and an apparent linear increase at greater wind speed. With respect to previous results (Wentz et al. 1986), a weak-wind speed (roughness-induced) linear portion is retained, and in moderate wind speeds, a quadratic shape is assumed where foam contributes to emission. This

function is fit using piecewise nonlinear least-squares to the emissivity and wind speed data:

$$\begin{aligned} \epsilon_w &= a_1 U_{sfc}, \quad U_{sfc} \leq w_l, \\ &= a_2 + a_3 U_{sfc} + a_4 U_{sfc}^2, \quad w_l < U_{sfc} \leq w_u, \\ &= a_5 + a_6 U_{sfc}, \quad U_{sfc} > w_u, \end{aligned} \tag{4}$$

where $w_l = 7 \ \mathrm{m\,s^{-1}}$, w_u is the objectively-determined knot point where the upper two curves meet, and the as are the fitted parameters. The model function is constrained such that the derivative is continuous across the knots, which results in the loss of two parameters. The upper knot location is found by identifying the minimum rms difference produced by the overall fit; trial w_us are tested from 20–50 $\mathrm{m\,s^{-1}}$. The best-fit parameters are found to be:

$$\begin{aligned} (a_1,\, a_2,\, a_3, a_4,\, a_5,\, a_6) &= (0.0401,\, 0.2866,\, -0.0418,\, 0.0058,\, -5.6658,\, 0.3314) \times 10^{-2}, \\ w_u &= 31.9 \,\mathrm{m\,s^{-1}}. \end{aligned}$$

Figure 4 shows the development dataset, along with the model function. The rms of the residuals is 0.011, around 10% of the mean at 50 $\mathrm{m\,s^{-1}}$.

[Figure 4 about here.]

To estimate the resultant wind speed uncertainty of the SFMR GMF, retrievals are computed from the SFMR measurements and correlated to the same U_{sfc} estimates used to develop the model function. The wind speed rms difference is found to be 3.6 $\mathrm{m\,s^{-1}}$. Uhlhorn and Black (2003) examined a number of contributions to this uncertainty, including variability in atmospheric and sea surface conditions, and found that the largest source of error in hurricanes was due to inaccurate sea surface temperature specification, especially at weak wind speeds ($< 20 \,\mathrm{m\,s^{-1}}$). Other sources of error may be due to inaccuracies of the rain absorption model, random instrument noise causing spurious solutions in the retrieval algorithm, and general spatial/temporal mis-location of measurement ground truth.

3. Evaluation Results

1) DEPENDENT SAMPLES

The improvement in SFMR retrieved wind speeds utilizing the new model function over the previous version is demonstrated in a number of ways. First, the retrievals obtained using the both new and old GMFs are compared for all 2005 SFMR-3 measurements (Fig. 5). As a majority (160/189) of the samples was used to develop the model function, these are not independent results. But this does illustrate the overall decrease in the GMF bias with respect to surface wind speed measurements. The resulting bias (–0.5 $\mathrm{m\,s^{-1}}$) is not found to be statistically significant based on a Student t-test.

[Figure 5 about here.]

An improvement is indicated by the near elimination of the moderate wind speed SFMR high bias (noted in Uhlhorn and Black (2003)), as well as the extreme wind underestimate. In developing the previous GMF, surface-adjusted flight-level winds speeds were increased by 10% (M. Powell, personal communication), based on the assumption that the extrapolated flight-level estimate represented a ∼10-min mean wind speed, whereas an estimate of the peak 1-min sustained wind speed was sought. The results here make no such assumption.

The previous GMF was derived using surface wind speed estimates no greater than 55 $\mathrm{m\,s^{-1}}$. Therefore, the uncertainty about the correct functional dependence at greater wind speeds was large. It is apparent here that the functional behavior at low-to-moderate wind speeds does not continue at extreme winds speeds, and the previous assumption to the contrary is likely responsible for the wind speed underestimate by SFMR. Based on these results, a linear increase in T_B with wind speed of ∼1.0 K/($\mathrm{m\,s^{-1}}$) is indicated for hurricane conditions, which is significantly greater than assumed in early SFMR studies. For example, Jones et al. (1981) used 0.7 K/($\mathrm{m\,s^{-1}}$) based on the results of Webster et al. (1976).

The results in Figure 5 generally indicate a greater degree of scatter at wind speeds higher than ∼30 $\mathrm{m\,s^{-1}}$, and is reflective of the GMF developmental data (Fig. 4). However, it is difficult to assess from these figures whether a majority of the variabilty lies in the SFMR or dropwindsonde measurements, as each contributes to the scatter. To examine the source of variability, error distributions are examined

separately for data plotted in Figure 5. For each set of data (SFMR-3 and U_{sfc}), wind speed measurements are sorted and detrended, and cumulative distributions below and above the 31.9 $\mathrm{m\,s^{-1}}$ GMF breakpoint are shown in Figure 6.

[Figure 6 about here.]

For low wind speeds (Fig. 6a), the dropwindsonde U_{sfc} data contribute significantly less variability than SFMR, based on a Kolmogorov-Smirnov test of the empirical cumulative distribution difference. At high winds (Fig. 6b), both data sets essentially contribute equally, as indicated by the distribution standard deviations.

A semi-independent demonstration of improvement is seen in HRD SFMR wind speed measurements for an expanded dataset obtained from N43RF flights (Figure 7). The residual scatter in the AOC SFMR retrievals is less than that from the HRD unit, such that the unexplained variability with respect to the GPS dropwindsonde ground truth is reduced by $\sim$1 $\mathrm{m\,s^{-1}}$. However, this is not a statistically significant improvement, as indicated by a Kolmogorov-Smirnov test.

[Figure 7 about here.]

2) INDEPENDENT EVALUATIONS

An independent test of the updated GMF is applied to surface wind speeds measured by SFMR-2 flown on N42RF. Unfortunately, no surface wind speeds were measured above 60 $\mathrm{m\,s^{-1}}$ in 2005 from this aircraft, so the extreme wind response cannot be independently evaluated. However, enough data were obtained at lower wind speeds to clearly demonstrate overall improvement (Figure 8). A t-test of the difference in mean bias between datasets processed with both the old and updated GMFs indicates significance at the 95% confidence level. A small, but statistically significant SFMR-2 high bias ($\sim$1.6 $\mathrm{m\,s^{-1}}$) using the new proposed GMF is noted which could be due to a slight calibration difference between the two operational SFMRs. in SFMR-2 was calibrated using measurements obtained over a broad ambient temperature (i.e. altitude) range, whereas SFMR-3 was calibrated at one altitude.

[Figure 8 about here.]

In Fig. 3, it was seen that the U_{sfc} estimate compared reasonably well with the actual measured 10-m wind speed (U_{10}). It is of interest to examine how well SFMR winds compare with U_{10}, as shown in Figure 9. Expectedly, the scatter is slightly enhanced in the SFMR-2 and SFMR-3 10-m correlations as compared to the results for U_{sfc}, but the bias is also affected, with a tendency for a slight decrease relative to the U_{sfc} results. This result is likely due to the small ($\sim$2%) average difference between U_{sfc} and U_{10} noted in the previous section.

[Figure 9 about here.]

4. Surface Wind Measurement Accuracy

With recent technological advances has come a fairly rapid growth in the quantity and type of near surface wind speed measurements in hurricanes. The GPS dropwindsonde has become an important tool to obtain surface wind velocity data, and airborne remote sensors, such as the SFMR, are increasingly used to measure surface quantities from a safe location. Often, numerous estimates of seemingly equivalent quantities are simultaneously available from different sources. In theory, increasing the number of observations of a random variable will improve measurement accuracy, but each datum has its own statistical characteristics, and utilizing multiple data sources for analysis often has the unintended consequence of *increasing* subjective uncertainty in a measurement. Additionally, remote sensing retrieval algorithms may require use of an empirical geophysical model function (GMF) that depends on external "ground-truth"; the derived model function therefore combines errors from multiple sensors.

In an operational hurricane forecast setting, data from multiple sources are often evaluated against one another to arrive at the best estimate of maximum surface wind speed. An attempt is made here to quantify individual measurement precision and accuracy of data sources that are typically used in conjunction with SFMR surface wind speed estimates. The two platforms of most interest here are surface-adjusted aircraft flight level and GPS dropwindsonde wind speeds. Recent research experiments have developed flight strategies to obtain measurements in a reasonably controlled environment to facilitate this assessment. Since a hurricane's intensity is defined by the maximum near-surface wind speed, the relationship between the peak SFMR-measured wind speed and conventional peak surface wind estimates is examined. Also,

we exploit the updated historical (1998-2005) SFMR dataset to identify the expected azimuthal location of the peak hurricane surface wind speed.

a. HSFMR vs dropwindsonde; flight-level winds

In 2003, a series of flights were conducted as part of the Office of Naval Research (ONR)-sponsored Coupled Boundary-Layer Air-Sea Transfer (CBLAST) experiment (Black et al. 2007). A major component of these flights was a number of "stair-step" patterns, flown by both WP-3Ds, designed to measure boundary layer profiles on the periphery of hurricanes. The flight patterns consisted of legs coordinated between the two aircraft. The higher aircraft (N42RF, $\sim$2100 m) deployed a series of GPS dropwindsondes along a single 40 km leg, while the lower aircraft (N43RF) performed repeated legs at varying heights (60–800 m) of the same length and at the same location. The lower WP-3D carried the HRD SFMR.

Ideally, wind measurements would have been obtained under stationary and horizontally homogeneous conditions, but some super turbulence-scale variability will inevitably exist. Patterns were flown in clear-air conditions, so measurements are largely free of convective motions and rainfall. Also, temperature profiles from GPS dropwindsondes indicate reasonably neutral stratification (potential temperature changes < 0.3 K) over the lowest 200–400 m of each profile. Four downwind and two crosswind coordinated profiles were obtained in Hurricanes Fabian and Isabel.

To generate statistics, 10-s averaged SFMR wind speeds are computed. GPS dropwindsonde statistics are also calculated for each set of sondes deployed by the higher-altitude aircraft – typically 3–4 sondes were dropped along a leg. For reference, flight-level statistical quantities are also estimated, although significant variability as a function of altitude would be expected. It is assumed that spatial and temporal variability on the scale of the sampled domain can be represented by a linear trend. Trends are identified separately for each type of data and subsequently removed prior to computing statistics. Figure 10 shows an example coordinated flight pattern and associated sonde profiles from one of six total patterns examined here, and Figure 11 shows corresponding SFMR and flight level wind speed time series'.

[Figure 10 about here.]

[Figure 11 about here.]

Statistics for the dropwindsonde 10-m wind measurement (U_{10}) and the near-surface estimate (U_{sfc}) are calculated, and normalized measurement variability (σ/μ) for each data source is shown in Table 2. HRD SFMR retrieved wind speed variability is around 5–8% of the mean, which is similar to that for U_{10}, and greater than that for U_{sfc} (1–5%). Under the assumption of stationarity and spatial homogeneity of the wind speed measurements, these values represent random measurement variability. Previous results from inter-comparisons of SFMR and dropwindsonde estimates indicate normalized rms differences of 10-15% at similar wind speeds (20–30 $\mathrm{m\,s^{-1}}$). This suggests that as much as 50% of the error in the GMF may be due to natural surface wind variability, further substantiating the results in Fig. 6, which indicate smaller rms errors in the individual data than in the derived GMF.

[Table 2 about here.]

b. HSFMR vs. AOC SFMR-3

The newer AOC operational SFMR theoretically contains a ∼50% lower noise-equivalent ΔT_B than does its predecessor. Unfortunately, not until 2005 were reliable measurements obtained simultaneously from both instruments, and flight patterns similar to those performed in 2003 were not executed due to experiment priorities. On the other hand, a flight pattern was flown as part of the NOAA Intensity Forecasting Experiment (IFEX) in which a single WP-3D (N43RF, with two SFMRs installed) flew extended legs parallel to, and outside of, rain bands. Numerous legs were flown during one particular flight (Hurricane Rita on 21 September 2005) under reasonably homogeneous and stationary conditions. These flights allowed a comparison of variability from both SFMRs.

A total of three flight legs of lengths 7, 13 and 10 minutes are used to compute wind speed statistics in identical fashion to the 2003 data. Time series of wind speeds from both SFMRs (SFMR-3 and HSFMR) and at flight level (∼3700 m) are shown in Fig. 12, and Table 3 gives error statistics for the measurements.

[Figure 12 about here.]

[Table 3 about here.]

The AOC SFMR produces wind speed measurements on average ∼50% less noisy than the HSFMR, which is simliar to the variability in U_{sfc} data from GPS dropwindsondes (2–4%). Again, these individual

error statistics are significantly smaller than the cross-compared samples of SFMR and GPS estimates (10–15%), which have been used to develop the GMF, as well as evaluate SFMR performance.

c. Estimating peak winds

Among the more important operational requirements of TPC/NHC is diagnosing the intensity of a hurricane in terms of the maximum sustained surface wind speed. Conventional methods of estimating this quantity from aircraft include extrapolating from flight level and utilizing pressure-wind relationships. The fairly recent advent of the GPS dropwindsonde has yielded direct measurements of near-surface wind speeds. Each of these estimates has their own limitations and we attempt here to demonstrate the added value of SFMR surface wind speed data in terms of reducing maximum wind speed uncertainty in hurricanes.

An evaluation of previously used flight-level-to-surface peak wind reductions is performed with respect to SFMR surface wind data. Numerous methods to estimate maximum wind speeds in TCs have been employed over time; current operational practice relies heavily on a relationship between GPS dropwindsonde near surface winds and aircraft measurements at standard reconnaissance flight levels (Franklin et al. 2003). The peak surface wind speed was found to be, on average, $\sim$90% of that at the 700 mb level, and $\sim$80% of the wind speed at 850 mb. Surface wind speed estimates are computed using these adjustment factors for eyewall penetrations during 2005 and correlated with the peak wind speed measured by GPS dropwindsonde along the same flight leg, as shown in Figure 13a, and compared with SFMR estimates (Fig. 13b).

[Figure 13 about here.]

Overall, a statistically-significant improvement by SFMR over the flight-level reduction method is indicated, with the largest differences in the 30-50 $\mathrm{m\,s^{-1}}$ range; comparable accuracy is found at extreme winds speeds. A fairly significant high bias in the flight-level reduced estimate relative to GPS dropwindsondes is shown (Fig. 13a), thus accounting for a 50% bias reduction improvement seen in the SFMR data. The "90% rule" is well confirmed for the *extreme* wind cases in this dataset, and considering the unexplained variability ($\pm 20\%$) in the results found by Franklin et al. (2003), applies reasonably well in

general. Interestingly, however, a significant underestimate (2.6 $\mathrm{m\,s^{-1}}$) by GPS dropwindsondes relative to SFMR (Fig. 13b) appears for *peak* wind speeds not present in the results obtained overall.

[Figure 14 about here.]

[Figure 15 about here.]

Figure 14 shows wind speeds as a function of radial distance from storm center for a typical eyewall aircraft penetration. Referring to Fig. 14, Figure 15a indicates a good correlation with minimal bias for the maximum U_{sfc} and SFMR measured at the sonde release, which is expected since these data were used to develop the GMF. However, as previously noted, a consistent low bias is found in the peak U_{sfc} with respect to the maximum SFMR wind speed (Fig. 15b). It is believed that the underestimate in the peak observed U_{sfc} relative to the peak observed SFMR wind speed is a result of the increased spatial coverage of SFMR measurements as compared to the typically single peak wind estimate from GPS dropwindsondes deployed in the eyewall. Figure 15c shows generally good correlation between peak SFMR and U_{10} from 20-60 $\mathrm{m\,s^{-1}}$, at the expense of expectedly increased scatter.

d. Surface peak wind location

Since a hurricane's intensity is defined by the maximum wind speed at any point in the storm, it is of interest to quantify the expected azimuthal location of the SFMR-measured earth-relative peak wind. Maximum 10-s average SFMR wind speeds (U_s) from 390 eyewall penetrations on 59 flights from 1998-2005 are found. For each measurement, the clockwise azimuth angle with respect to the direction of storm motion (θ) is calculated. A wavenumber $n = 1$ (per 2π radians) asymmetric trigonometric function of the form:

$$U_s = \alpha_0 + \alpha_1 \cos(\theta + \alpha_2) \tag{5}$$

is fit to the data for each flight. The rms error of each fit is calculated, and fits with >10% error about the mean (α_0) are rejected. A total of 49 cases are accepted. An example from Hurricane Rita on 22 September 2005 is shown in Figure 16.

[Figure 16 about here.]

The expected SFMR peak wind phase is located at $\theta = -\alpha_2$. Peak phase estimates are binned into 30° intervals, and the peak wind speed location frequency distribution is shown in Figure 17. Additionally, the frequency distributions for minimal (SS category 1/2) and major (category 3/4/5) hurricanes are also plotted.

[Figure 17 about here.]

The peak SFMR wind speed is found to be located roughly 40° clockwise from the storm motion direction, on average. Also, the peak is located in the right-front storm quadrant ($0 < \theta < 90°$) in around 50% of the cases, and is in the right-rear quadrant approximately 25% of the time. For intense hurricanes, the peak wind right-front quadrant frequency increases to almost 65%. These results are consistent with previous observations (Powell 1982) and theoretical results (Shapiro 1983; Kepert 2001) concerning the spatial distribution of boundary-layer winds.

The location of the peak depends partly on the storm's translation speed, and is due to enhanced nonlinear asymmetric advective interactions as speed increases (Shapiro 1983). A fairly clear tendency emerges (not shown), such that the SFMR peak location rotates ∼8° clockwise for each $\mathrm{m\,s^{-1}}$ increase in forward speed. Based on this limited sample, the SFMR peak wind speed is found in the right-rear quadrant for hurricanes translating faster than ∼11 $\mathrm{m\,s^{-1}}$. It is important to note that several other factors may control the peak wind location, such as the environmental shear in which a hurricane is embedded, spatial variability of sea surface conditions, and frictional effects due to coastal proximity.

5. Discussion

In developing the previous GMF, the wind-induced surface emissivity was calculated and correlated with simultaneous surface wind speed estimates extrapolated from flight-level (500 m) winds using the boundary-layer model of Powell (1980). Fundamentally, the model assumes that the neutral stability wind profile, $U(z)$, from flight level to the surface has a logarithmic shape. The slope in log-height coordinates is proportional to the friction velocity (u_*), and intercept is determined by the surface roughness length (z_0), *viz.*:

$$U(z) = \frac{u_*}{k} \ln\left(\frac{z}{z_0}\right), \tag{6}$$

where k is the von Karman constant. Closure is achieved by relating u_* and z_0 by dimensional argument through a Charnok (1955) expression. Errors in these quantities (or in the assumed shape) will, of course, induce biases in extrapolated surface wind speeds. For example, if the observed roughness is smaller than predicted, one might expect a relatively higher surface wind speed extrapolation from flight-level.

A recent analysis of GPS dropwindsonde wind speed profiles in the hurricane inner core (Franklin et al. 2003) indicated that surface (10-m) winds were, on average, around 88% of the wind speed at 700 mb ($\sim$3100 m). This value is roughly 10% greater than predicted by traditional BL models. Franklin et al. (2003) speculated that convective transport of momentum downward toward the surface was responsible for this momentum excess in the eyewall BL. The Powell et al. (2003) study yielded essentially identical results, and demonstrated the observed weak slope of the logarithmic wind profile produced a lower drag coefficient and roughness length than previously assumed. This conclusion suggests less of a frictional drain on momentum in TC conditions.

With the recent ONR-sponsored CBLAST experiment, attention has turned toward gaining a better understanding of air-sea momentum exchange in hurricanes. Data from both laboratory experiments (Donelan et al. 2004) and field measurements (French et al. 2006) generally agree that the scalar momentum exchange (drag) coefficient, $C_d \equiv (u_*/U)^2$, does not continue to increase in hurricane force winds speeds as it does at weaker winds. Previous boundary layer models that have assumed an extrapolation of low-wind C_d behavior to hurricane speeds would have a tendency to underestimate surface wind speeds extrapolated from flight level. This is likely the reason for the initial bias in extreme SFMR surface wind speed estimates utilizing the previously-developed GMF; excess emissivity measurements in these conditions were correlated to surface wind speeds which were on average underestimated.

The laboratory results of Donelan et al. (2004) present compelling evidence that the physical nature of the air-sea interface is markedly altered when wind speeds exceed hurricane force. The overall effect is to reduce the downward flux of kinetic energy to the sea surface relative to what would be expected if the low-wind speed behavior continued at higher wind speeds. Field observations of GPS dropwindsonde wind profiles agree with this hypothesis, as the extrapolated roughness lengths are shown to be significantly lower than previously expected. Though not directly related to the surface roughness and drag, the SFMR's emissivity measurements also corroborate these results.

The excess emissivity is a function of the foam coverage, which is produced mainly by breaking surface waves. Thus the emissivity is more directly related to surface wave energy dissipation, S_D, and *not* wind energy input, S_W. These two quantities are related through the surface wave energy balance, which can simply be expressed as:

$$\frac{1}{E}\frac{dE}{dt} = S_W - S_D + S_N, \tag{7}$$

where $E = E(\vec{k},\, \theta;\, \vec{x},\, t)$ is the two-dimensional energy spectrum and S_N represents non-linear interactions among spectral components. The energy input is related to the wind by (Terray et al. 1996):

$$S_W \sim \overline{c}\, u_*^2, \tag{8}$$

where $\overline{c}$ is a characteristic wave phase speed. In the theoretical deep-water equilibrium limit, growth is arrested, and $S_W = S_D$. Thus the growth of wind waves and spectral interaction prevents a unique relationship between the surface wind speed and emissivity in all sea-state conditions. Following this interpretation, Uhlhorn and Black (2003) noted a small ($\sim$2.5 $\mathrm{m\,s^{-1}}$) azimuthal (with respect to TC motion direction) modulation of SFMR wind retrieval errors, and attributed this result to the strong variation in fetch length and duration in a TC. If S_W is, on average, smaller than expected due to a lower u_* (or C_d) for the same wind speed, there should also be a compensating decrease in S_D to maintain the energy balance. It appears that at around the same point where C_d levels off, the low-wind ($<$32 $\mathrm{m\,s^{-1}}$) quadratic increase in excess emissivity ceases, and a more modest linear increase is observed (Fig 4).

6. Conclusions

The new NOAA/AOC Stepped Frequency Microwave Radiometer represents a potentially significant advancement in remote measurement of hurricane near-surface wind speeds, most notably in speeds $>$50 $\mathrm{m\,s^{-1}}$. This improvement is due to both refined remote-sensing technologies, and more accurate ground-truth data in the form of GPS dropwinsonde wind speed measurements. The AOC SFMR yields wind speed measurements overall within $\sim$4 $\mathrm{m\,s^{-1}}$ rms of the dropwindsonde-estimated surface wind, and within $\sim$5 $\mathrm{m\,s^{-1}}$ of the direct 10-m wind speed measurement. Wind speed measurements from the con-

temporary AOC SFMR show precision better than the Hurricane Research Division's SFMR by around a factor of two.

The observation of a linear increase in sea surface emissivity with wind speed at hurricane-force is a shift in understanding about sea surface radiometric properties. In practical terms, the previous quadratic emissivity/wind speed model consistently underestimated winds at speeds $>50\ \mathrm{m\,s^{-1}}$, and the new linear GMF corrects this anomaly. From a scientific standpoint, additional evidence is found for a distinct physical change in the sea surface when surface winds exceed $\sim 30\ \mathrm{m\,s^{-1}}$, and further, that momentum and kinetic energy exchanges are relatively reduced at high wind speeds. This gain in understanding potentially will lead to improvements in air/sea exchange parameterizations, ultimately resulting in superior hurricane intensity forecasts.

With the recent spate of North Atlantic basin major hurricanes and the expected continuation of elevated activity, accurate intensity diagnosis is crucial for improved coastal watches/warnings and more efficient evacuations. The anticipated installation of SFMRs aboard Air Force Reserve Command (AFRC) hurricane reconnaissance aircraft will greatly increase the frequency at which storms are observed by SFMR, and additional future algorithm modifications utilizing concomitant precipitation data from advanced airborne radars are expected to further improve SFMR hurricane wind speed accuracy.

Acknowledgement

The authors acknowledge Prof. Calvin T. Swift (U. of Massachusetts) for the SFMR concept, and Richard F. Harrington (formerly NASA/LaRC) for the original instrument design. We thank the Office of the Federal Coordinator for Meteorology (OFCM), and especially Robert J. Dumont and OFCM director Samuel P. Williamson, for sustained support and funding of the HRD SFMR instrument over the years, and recently for the AOC opererational SFMRs. We thank TPC/NHC Director Max Mayfield for continued support of SFMR and NHC Hurricane Specialists for their valuable feedback. Specifically, we thank NHC forecasters Stacy Stewart and Jamie Rhome for their insightful reviews. The expertise and cooperation of NOAA/AOC flight program manager Dr. James D. McFadden, and AOC engineers and flight crew are greatly appreciated. Finally, we acknowledge Drs. Sim Aberson, Robert Rogers, Mark Powell (HRD), and two anonymous reviewers for their constructive comments on the original manuscript.

References

Black, P. G., E. A. D'Asaro, W. Drennan, J. French, P. Niiler, T. Sanford, E. Terrill, E. Walsh, and J. Zhang, 2007: Air-sea exchange in hurricane winds: Synthesis of observations from the Coupled Boundary Layer Air-Sea Transfer Experiment. *Bull. Am. Meteor. Soc.*, In press.

Black, P. G. and C. L. Swift, 1984: Airborne stepped frequency microwave radiometer measurements of rainfall rate and surface wind speed in hurricanes. *Preprints, 2nd Conf. on Radar Meteor.*, Amer. Meteor. Soc., Zurich, Switzerland, 433–438.

Blackadar, A. K., 1965: A simplified two-layer model of the baroclinic neutral atmospheric boundary layer. Final Report: Flux of heat and momentum in the planetary boundary layer of the atmosphere. Technical report, The Pennsylvania State University, State College, PA.

Cardone, V. J., 1969: Specification of the wind distribution in the marine boundary layer for wave forecasting. Technical Report TR69-1, Dept. of Meteorology and Oceanography, New York University, New York, NY.

Charnok, H., 1955: Wind stress on a water surface. *Q. J. R. Met. Soc.*, **8**, 639–640.

Deardorff, J. W., 1972: Parameterization of the planetary boundary layer for use in general circulation models. *Mon. Wea. Rev.*, **100**, 93–106.

Donelan, M. A., B. K. Haus, N. Reul, W. J. Plant, M. Stiassnie, and H. C. Graber, 2004: On the limiting aerodynamic roughness of the ocean in very strong winds. *Geophys. Res. Lett.*, **31**, doi:10.1029/2004GL019460.

Dunion, J. P., C. W. Landsea, S. H. Houston, and M. D. Powell, 2003: A reanalysis of the surface winds for Hurricane Donna of 1960. *Mon. Wea. Rev.*, **131**, 1992–2011.

Franklin, J. L., M. L. Black, and K. Valde, 2003: GPS dropwindsonde wind profiles in hurricanes and their operational implications. *Wea. Forecasting*, **18**, 32–44.

French, J. R., W. M. Drennan, J. Zhang, and P. G. Black, 2006: Turbulent fluxes in the hurricane boundary layer. Part I: Momentum flux. *J. Atmos. Sci.*, In press.

Goodberlet, M. A. and J. B. Mead, 2006: Two-load radiometer precision and accuracy. *IEEE Trans. Geosci. Rem. Sens.*, **44**, 58–67.

Goodberlet, M. A., C. T. Swift, and J. C. Wilkerson, 1989: Ocean surface wind speed measurements of the Special Sensor Microwave/Imager (SSM/I). *J. Geophys. Res.*, **94**, 14547–14555.

Hock, T. F. and J. L. Franklin, 1999: The NCAR GPS dropwindsonde. *Bull. Amer. Meteor. Soc.*, **80**, 407–420.

Holland, P. W. and R. E. Welsch, 1977: Robust regression using iteratively reweighted least-squares. *Communications in Statistics - Theory and Methods*, **A6**, 813–827.

Jiang, H., P. G. Black, E. J. Zipser, F. D. Marks Jr., and E. W. Uhlhorn, 2006: Validation of rain rate estimation in hurricanes from the stepped frequency microwave radiometer: Algorithm correction and error analysis. *J. Atmos. Sci.*, **63**, 252–267.

Jones, W. L., P. G. Black, V. E. Delnore, and C. T. Swift, 1981: Airborne microwave remote-sensing measurements of Hurricane Allen. *Science*, **214**, 274–280.

Jordan, C. L., 1958: Mean soundings for the West Indies area. *J. Meteor.*, **15**, 91–92.

Jorgensen, D. P. and P. L. Willis, 1982: A $Z - R$ relationship for hurricanes. *J. Appl. Meteor.*, 356–366.

Kepert, J., 2001: The dynamics of boundary layer jets within the tropical cyclone core. Part I: Linear theory. *J. Atmos. Sci.*, **58**, 2469–2484.

Klein, L. A. and C. A. Swift, 1977: An improved model for the dialectric constant of sea water at microwave frequencies. *IEEE J. Oceanic Engr.*, **OE-2**, 104–111.

Olsen, R. L., D. V. Rogers, and D. B. Hodge, 1978: The aR^b relation in the calculation of rain attenuation. *IEEE Trans. Antennas Propagat.*, **AP-26**, 318–329.

Powell, M. D., 1980: Evaluations of diagnostic marine boundary layer models applied to hurricanes. *Mon. Wea. Rev.*, **108**, 757–766.

— 1982: The transition of the Hurricane Frederic boundary-layer wind field from the open Gulf of Mexico to landfall. *Mon. Wea. Rev.*, **110**, 1912–1932.

Powell, M. D., T. A. Reinhold, and R. D. Marshall, 1999: GPS sonde insights on boundary layer wind structure in hurricanes. *Preprints, 10th Intl. Conf. Wind Engr.*, A. Larsen, G. L. Larose, and F. M. Livesey, eds., Copenhagen, Denmark, 307–314.

Powell, M. D., P. J. Vickery, and T. A. Reinhold, 2003: Reduced drag coefficient for high wind speeds in tropical cyclones. *Wea. Forecasting*, **18**, 32–44.

Shapiro, L. J., 1983: The asymmetric boundary layer flow under a translating hurricane. *J. Atmos. Sci.*, **40**, 1984–1998.

Swift, C. T., D. C. DeHority, P. G. Black, and J.-Z. Chein, 1984: Microwave remote sensing of ocean surface wind speed and rain rates over tropical storms. *Frontiers of remote sensing of the oceans and troposphere from air and space platforms*, NASA, Shoresh, Israel, 281–286.

Tanner, A. C., C. T. Swift, and P. G. Black, 1987: Operational airborne remote sensing of wind speeds in hurricanes. *Preprints, 17th Conf. Hurr. and Trop. Meteor.*, Amer. Meteor. Soc., Miami, FL, 385–387.

Terray, E. M., M. A. Donelan, Y. C. Agrawal, W. M. Drennan, K. K. Kahma, A. J. Williams III, P. A. Hwang, and S. A. Kitaigorodskii, 1996: Estimates of kinetic energy dissipation under breaking waves. *J. Phys. Oceanogr.*, **26**, 792–807.

Uhlhorn, E. W. and P. G. Black, 2003: Verification of remotely sensed sea surface winds in hurricanes. *J. Atmos. Oceanic Tech.*, **20**, 99–116.

Ulaby, F. W., R. K. Moore, and A. K. Fung: 1981, *Microwave Remote Sensing, Active and Passive*, volume 1. Artech House, Inc., 456 pp.

Webster, W. J. J., T. T. Wilheit, D. B. Ross, and P. Gloerson, 1976: Spectral characteristics of the microwave emission from a wind-driven foam-covered sea. *J. Geophys. Res.*, **81**, 3095–3099.

Wentz, F. J., 1983: A model function for ocean microwave brightness temperatures. *J. Geophys. Res.*, **88**, 1892–1908.

Wentz, F. J., L. A. Mattox, and S. Peteherych, 1986: New algorithms for microwave measurements of ocean winds: Applications to SEASAT and the Special Sensor Microwave Imager. *J. Geophys. Res.*, **91**, 2289–2307.

List of Figures

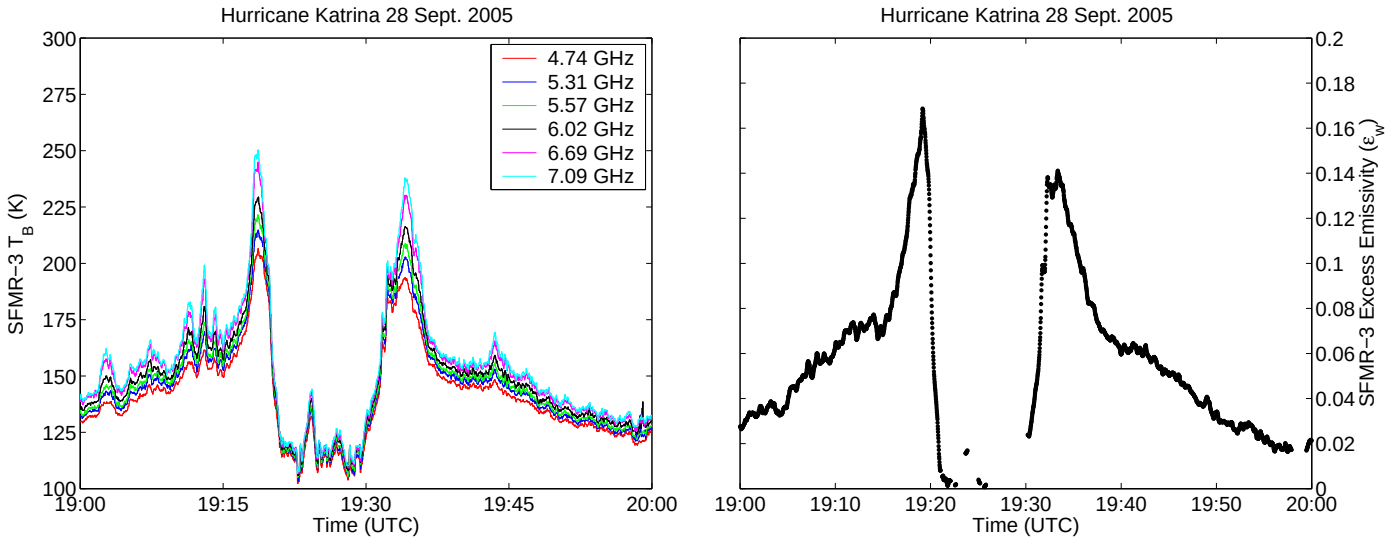

Figure 1: Time series (radial cross section) of T_B measurements for each SFMR channel from Hurricane Katrina (left panel), and the corresponding mean frequency-independent, wind-induced, excess emissivity (right panel).

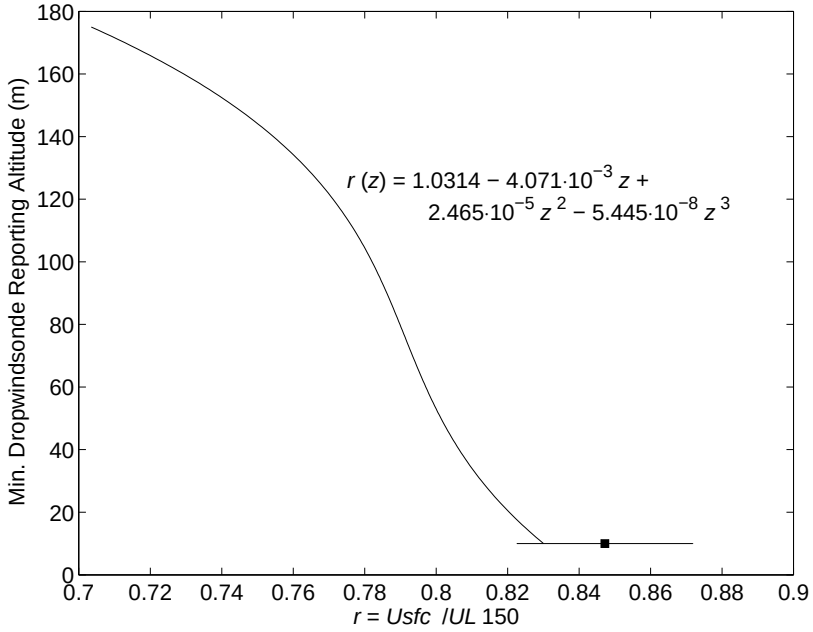

Figure 2: Ratio $r(z)$ of GPS dropwindsonde near-surface wind speed (U_{sfc}) to lowest 150-m average wind speed (U_{L150}) empirically determined from a mean eyewall profile developed by Franklin et al. (2003). For comparison, $r(z = 85\,\mathrm{m}) = 0.85 \pm 0.03$ found here (Fig. 3a) is indicated by the single data point.

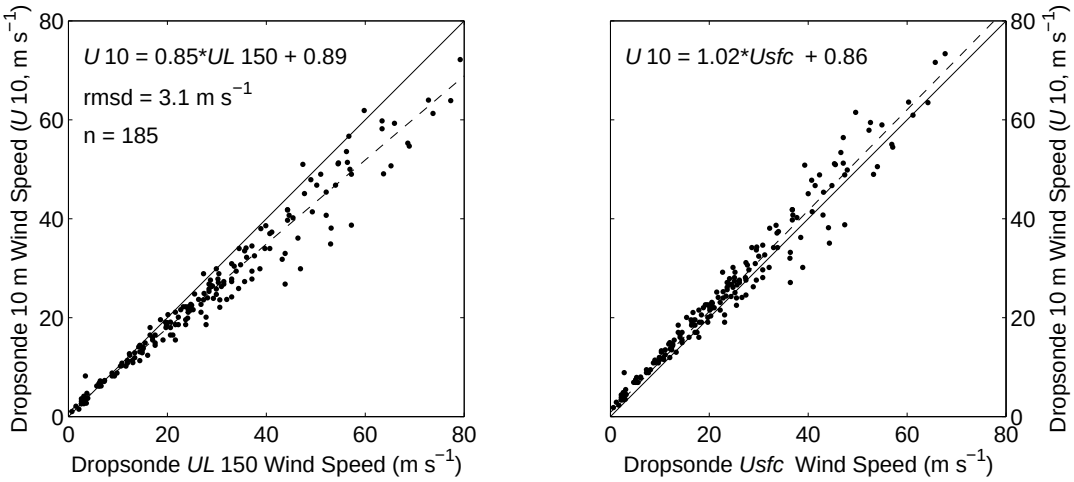

Figure 3: Surface winds measured by GPS dropwindsondes used for GMF development. The left panel shows GPS 10 m wind speed (U_{10}) plotted vs. U_{L150}, and the right panel shows U_{10} vs. U_{sfc} estimated using the eyewall-based surface adjustment method.

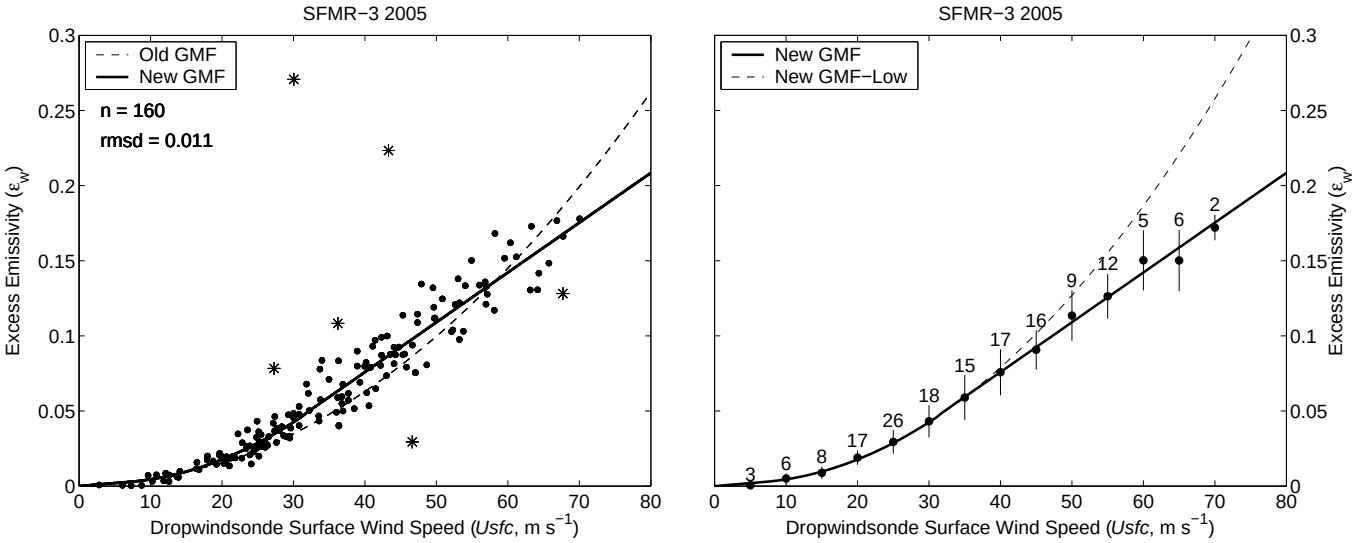

Figure 4: Wind induced excess emissivity (ϵ_w) as a function of U_{sfc} (left panel), and binned ϵ_w estimates (right panel). In the left panel, the best-fit result (Equation 5) is plotted as "New GMF", and the previous quadratic model function ("Old GMF") is shown as the dashed line for comparison. The six points rejected by the outlier detection are plotted as asterisks. In the right panel, the low wind speed quadratic portion of the new GMF ("New GMF-Low") is shown extended to the high-wind region to highlight the distinct behavior difference below and above $\sim 32\ \mathrm{m\,s^{-1}}$. Errorbars are 1σ, and values are number of observations per bin.

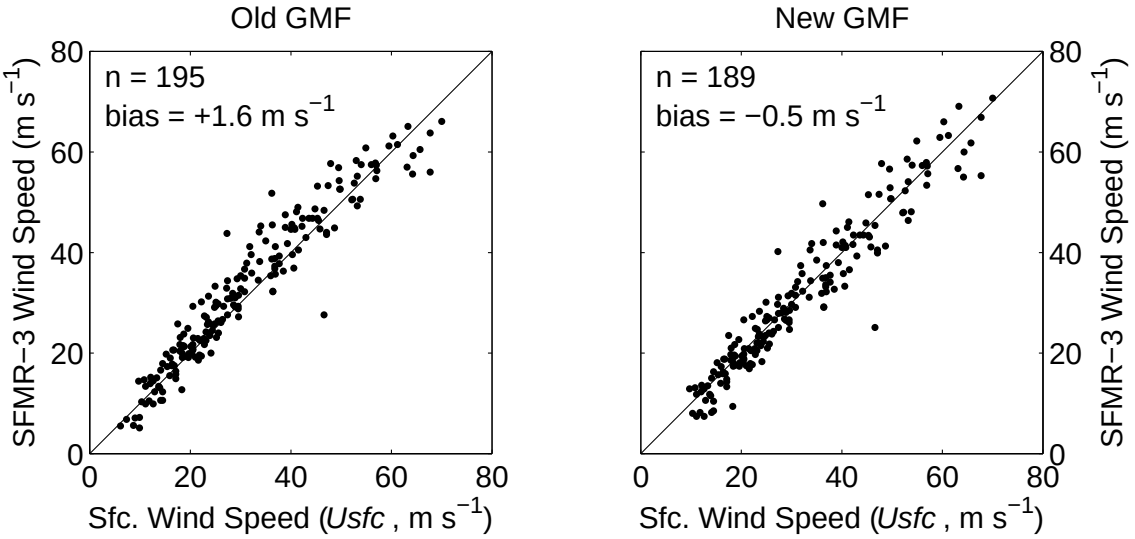

Figure 5: AOC SFMR-3 surface winds vs. U_{sfc} for all dropwindsonde data obtained after July 2005. Left panel uses old GMF, right panel uses new GMF. Note that the number of SFMR retrievals is different for each GMF, since each function has unique convergence properties at weak wind speeds where sensitivity is lowest.

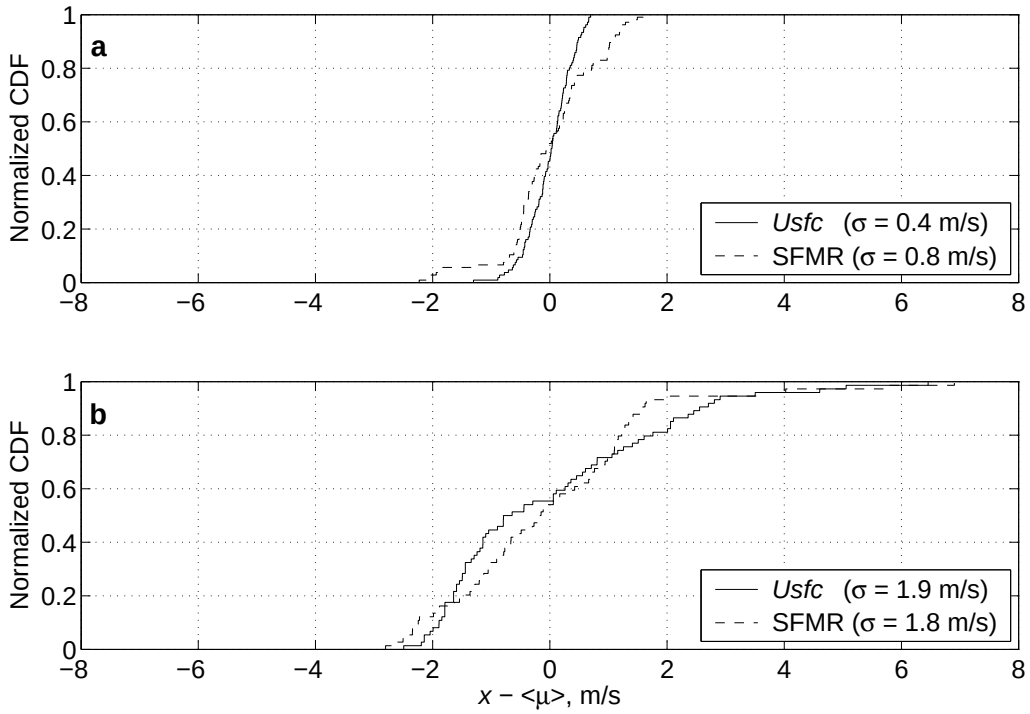

Figure 6: Normalized cumulative distributions of sorted/detrended surface wind speed data $\leq$31.9 $\mathrm{m\,s^{-1}}$ (a) and $>$31.9 $\mathrm{m\,s^{-1}}$ (b).

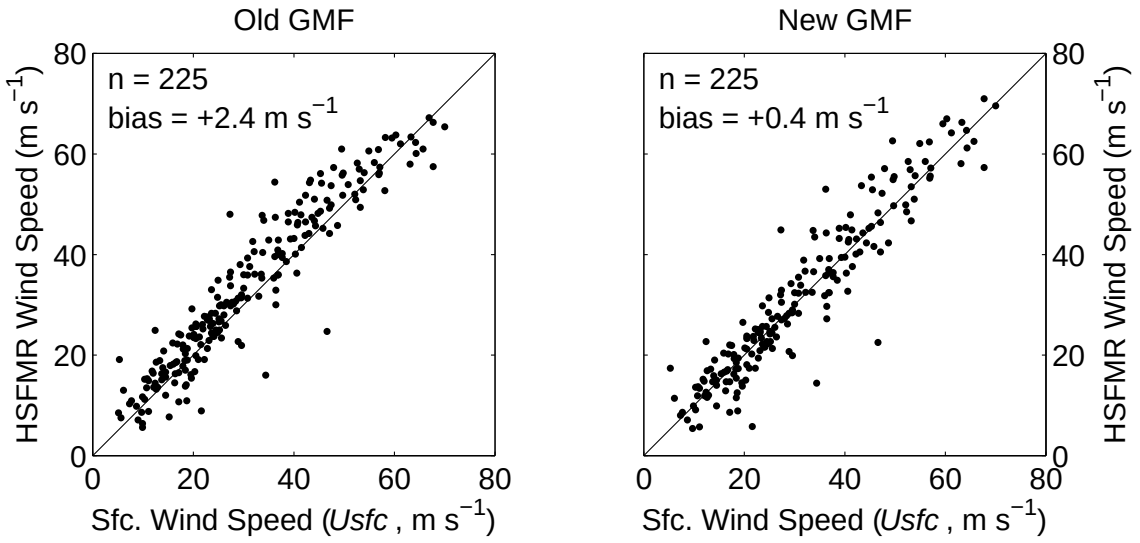

Figure 7: Same as Fig. 5, but for HRD SFMR and for data collected over entire 2005 season.

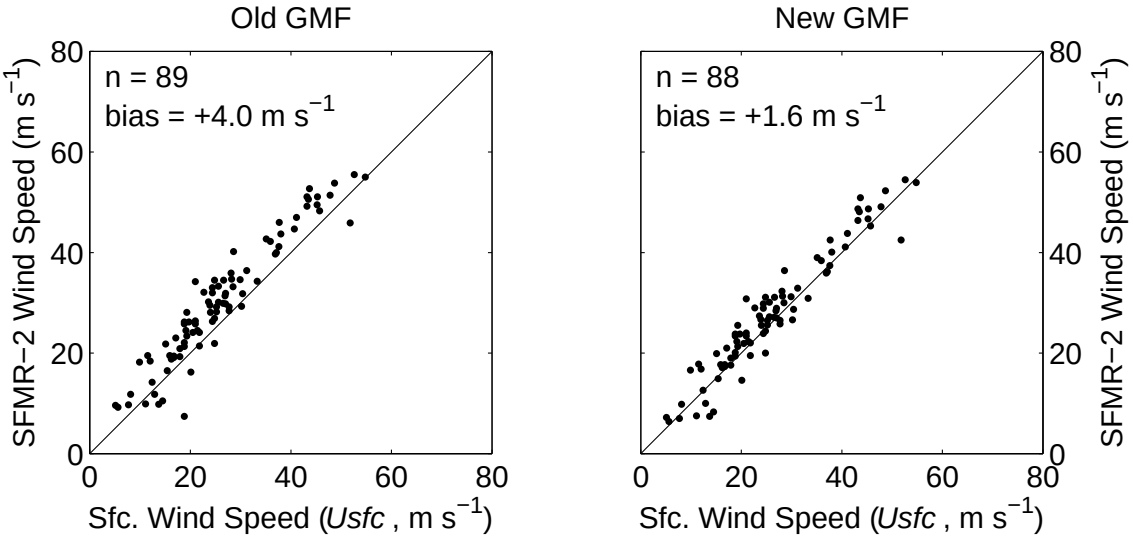

Figure 8: Same as Fig. 5, but for SFMR-2 data collected over entire 2005 season.

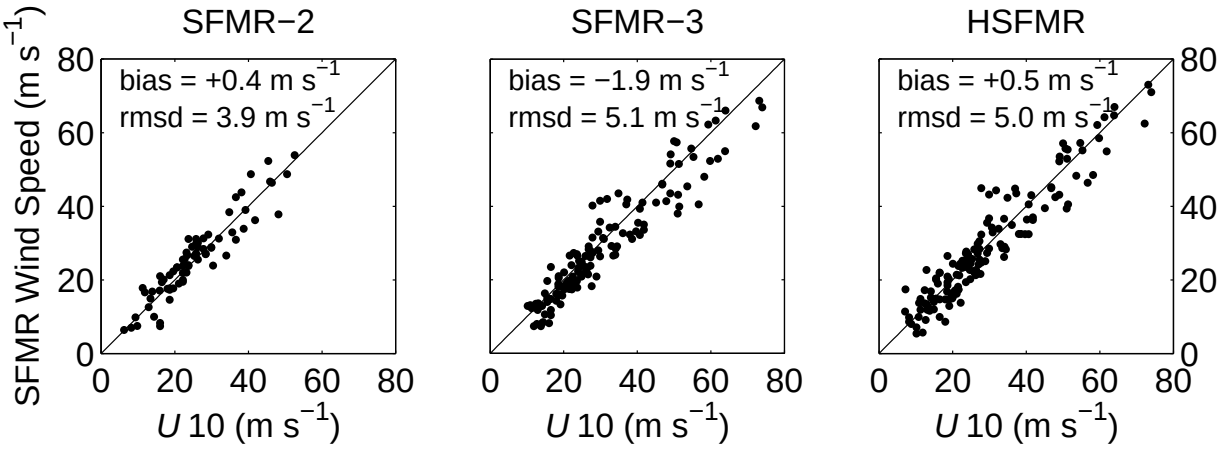

Figure 9: Surface wind speed retrievals vs. U_{10} for all 3 SFMRs.

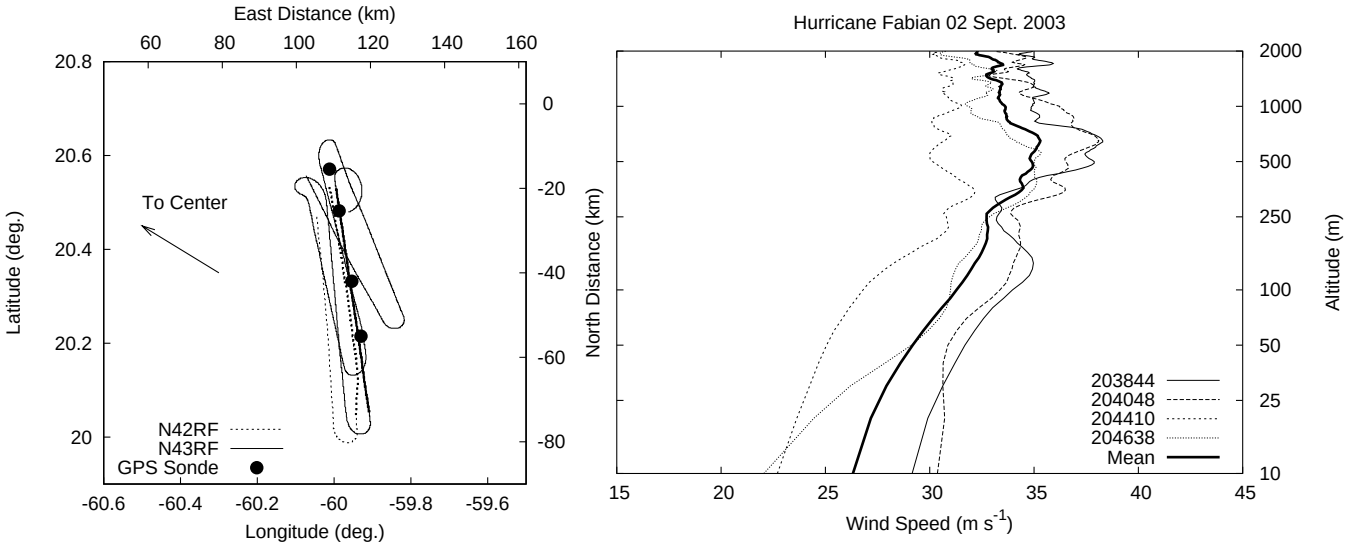

Figure 10: Coordinated WP-3D flight patterns along with GPS dropwindsonde splash locations (left panel) and dropwindsone wind speed profiles in Hurricane Fabian. Thicker lines in left panel represent period over which statistics are estimated. GPS sondes are labeled by UTC launch time (HHMMSS).

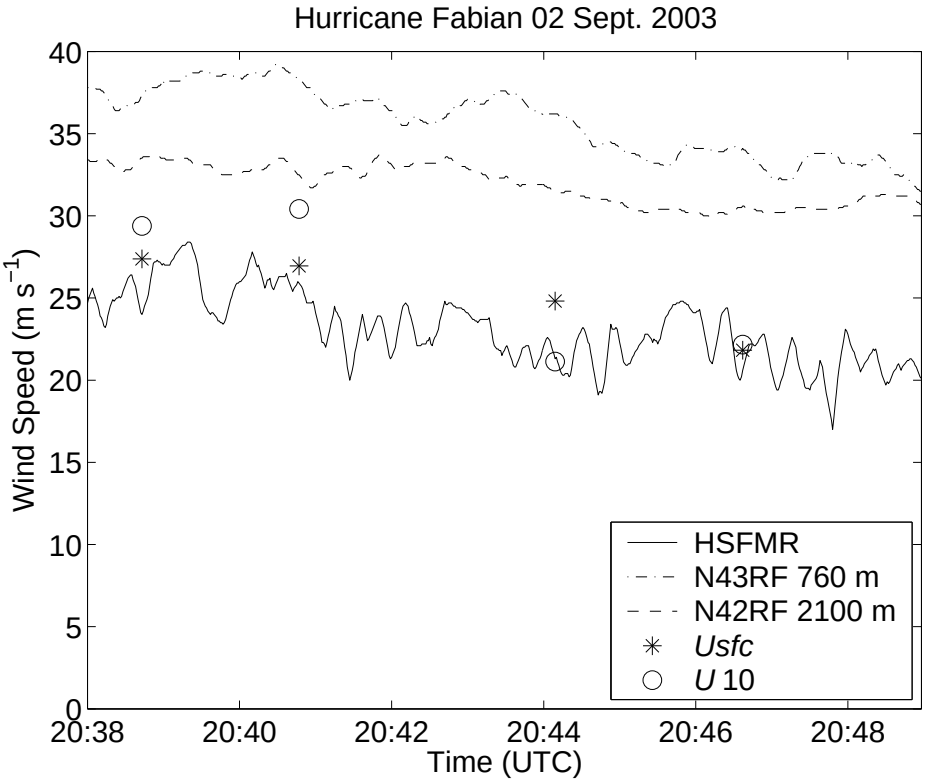

Figure 11: Time series of winds for P-3 coordinated flight pattern example shown in Figure 10, along with GPS surface wind estimates.

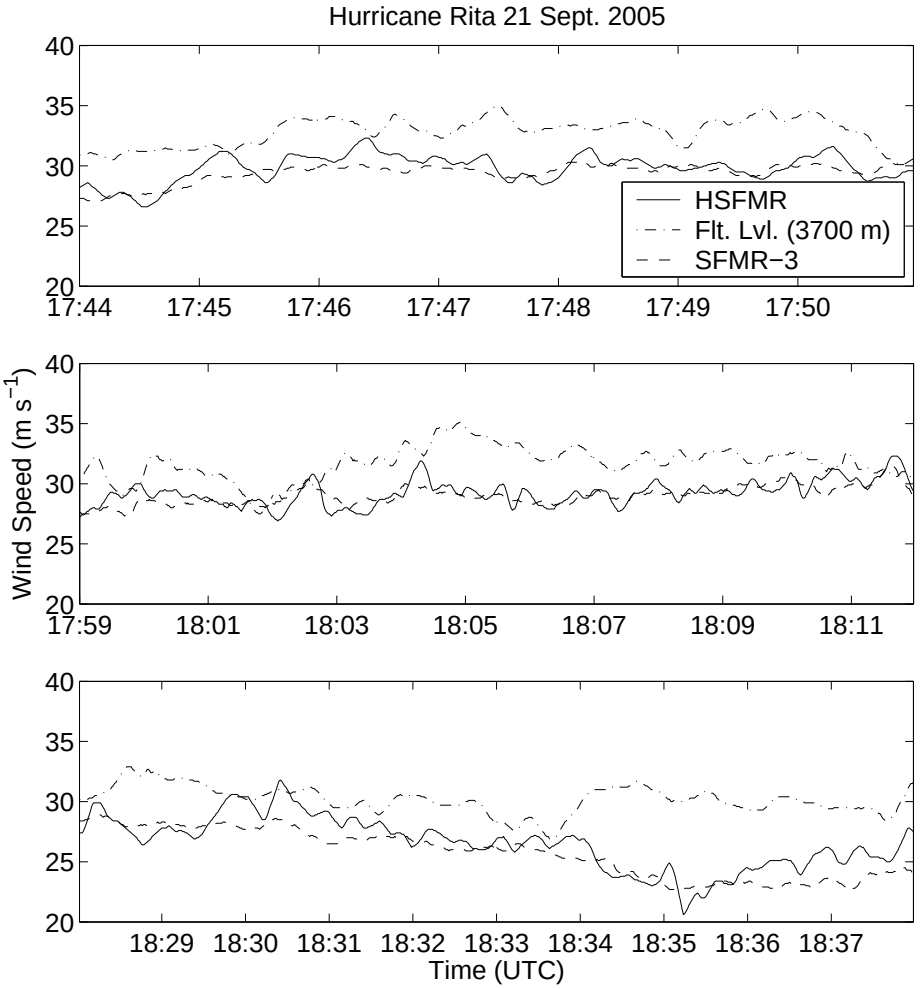

Figure 12: Time series of wind measurements for three segments from both SFMRs installed on N43RF, along with flight-level (∼3700 m) wind speeds.

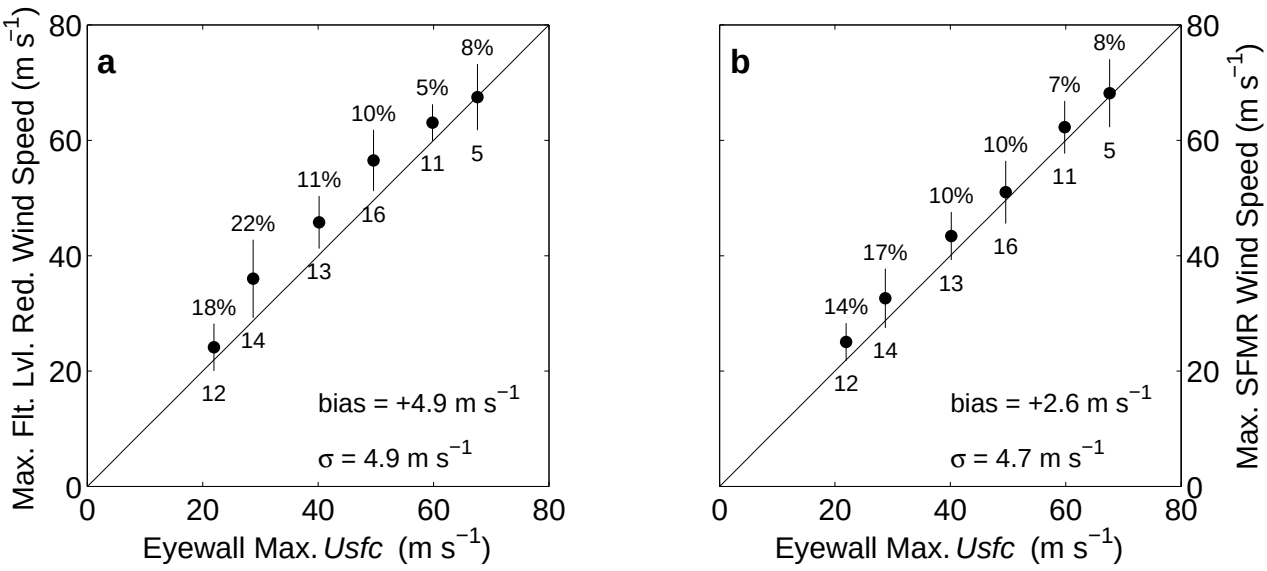

Figure 13: Peak GPS surface wind (U_{sfc}) measured on a flight leg vs. peak surface wind estimated from flight level data (a), and vs. peak SFMR wind speed (b). Mean values are computed over 10 $\mathrm{m\,s^{-1}}$ bandwidths, and errorbars are 1 standard deviation. Values below errorbars are number of samples per bin, and values above indicate relative uncertainty ($\%$). Overall statistics are also presented for each comparison.

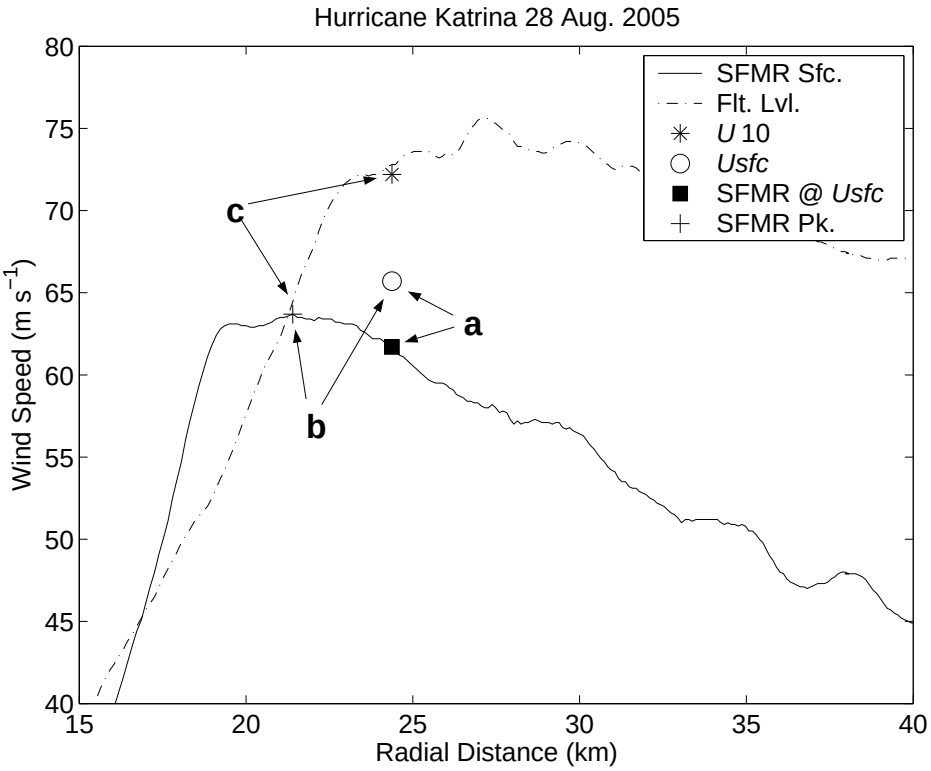

Figure 14: Winds vs. radial distance from center for a typical aircraft eyewall penetration. Letters correspond to panels in Figure 15 and refer to the data pairs examined.

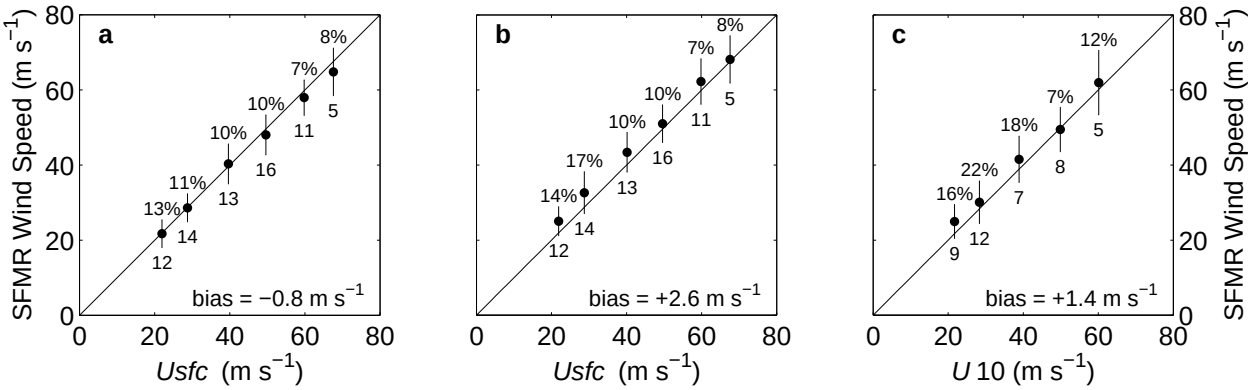

Figure 15: Maximum GPS surface wind speed (U_{sfc}) vs SFMR at sonde release point (panel a); U_{sfc} vs. peak SFMR wind (b); and maximum GPS 10-m wind (U_{10}) vs. peak SFMR (c). Panels correspond to data points indicated in Fig. 14.

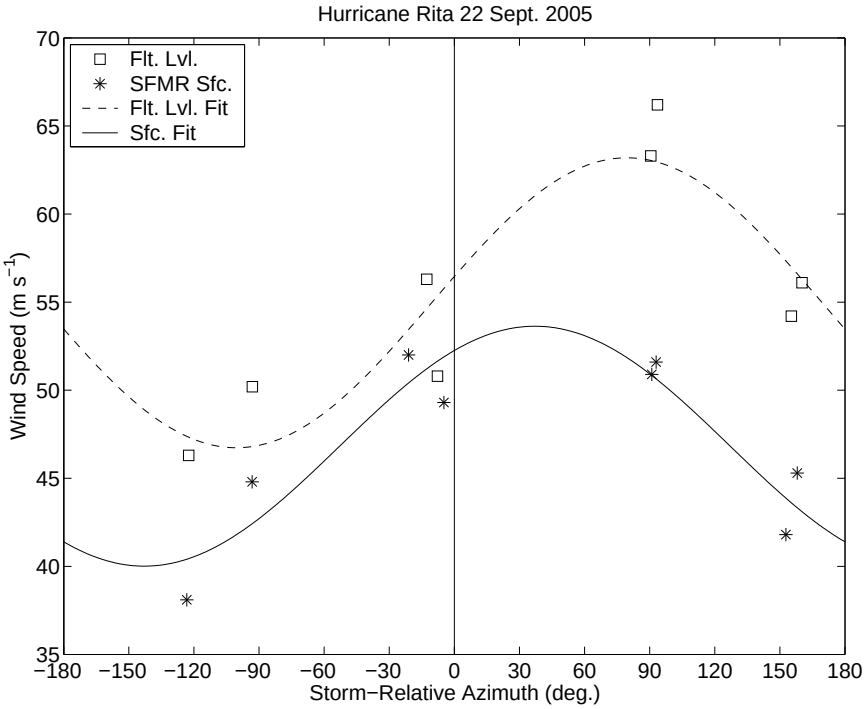

Figure 16: Surface and flight-level wind speeds as a function of clockwise azimuth angle with respect to storm motion direction. Also shown are wavenumber 1 fits to the data based on Equation 5.

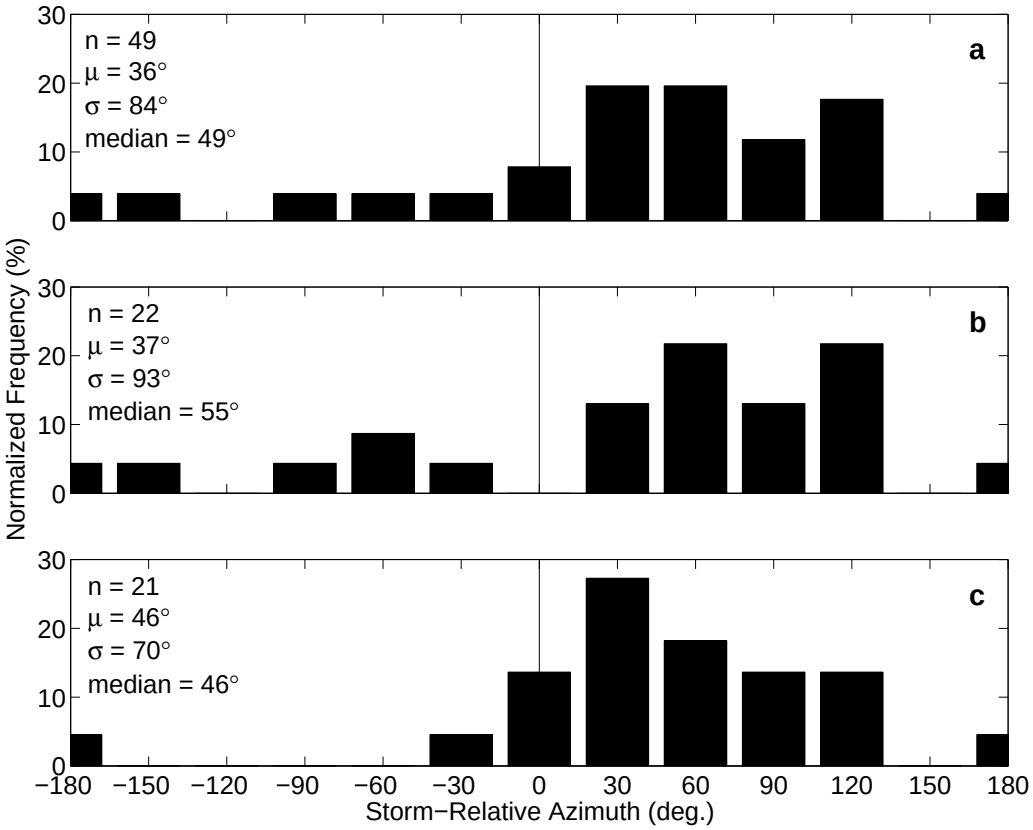

Figure 17: Frequency distribution of peak surface wind speed phase for all storms (panel a), for category 1/2 hurricanes (b) and for major category 3/4/5 hurricanes (c). The storm motion direction is at 0°. The peak wind speed is typically located in the right-front quadrant of a storm.

List of Tables

Storm	Flight ID	# Sondes	# $U_{sfc} > 50$ $\mathrm{m\,s^{-1}}$	# $U_{sfc} > 60$ $\mathrm{m\,s^{-1}}$
Katrina	20050825I	9	0	0
Katrina	20050827I	22	0	0
Katrina	20050828I	33	11	5
Katrina	20050829I	23	0	0
Rita	20050921I	28	10	6
Rita	20050922I	30	6	0
Rita	20050923I	41	0	0

Table 1: Summary of flights from which measurements were taken to develop the new $\epsilon_w = f(U_{sfc})$ GMF. Flight ID is date and aircraft (I = N43RF). The number of sondes refers to the potential number of paired SFMR emissivity/GPS sonde samples prior to outlier screening.

Data Source	Variability (%)
Flt. Lvl. ($\sim$2100 m)	2.8 ± 1.3
Flt. Lvl. ($\sim$350 m)	3.5 ± 1.5
U_{sfc}	2.0 ± 2.3
U_{10}	6.2 ± 5.1
HSFMR	6.5 ± 1.8

Table 2: Summary of normalized random variability for wind measurements obtained for the six 2003 CBLAST coordinated flight patterns in Hurricanes Fabian and Isabel.

Data Source	Variability (%)
Flt. Lvl. ($\sim$3700 m)	3.7 ± 0.5
HSFMR	4.1 ± 1.4
AOC SFMR-3	2.2 ± 0.4

Table 3: Statistical summary of normalized random variability for wind measurements shown in Figure 12 in Hurricane Rita on 21 September 2005.